Coherent versus noncoherent Bloch oscillations in the presence of direct and alternating fields

E. Ben-Jacob
School of Physics and Astronomy, Raymond and Beverly Sackler Faculty of Exact Sciences, Tel-Aviv University, 69 978 Tel-Aviv, Israel
and Department of Physics, University of Michigan, Ann Arbor, Michigan 48109-1120

Y. Gefen*
Department of Physics, (FM-19), University of Washington, Seattle, Washington 98195

K. Mullen
Department of Physics, University of Michigan, Ann Arbor, Michigan 48109-1120

Z. Schuss
School of Mathematics, Raymond and Beverly Sackler Faculty of Exact Sciences, Tel-Aviv University, 69 978 Tel-Aviv, Israel
(Received 17 December 1986; revised manuscript received 2 October 1987)

We first study noncoherent Bloch oscillations in ultrasmall-capacitance normal tunnel junctions using the semiclassical approach. We then study coherent Bloch oscillations in other systems showing an energy spectrum similar to the "nearly-free-electron" model in the extended–Brillouin-zone picture, and compare the two pictures. In the latter we calculate the response to a constant driving force, including both Zener tunneling and inelastic transitions between the energy bands. For both cases we also calculate the response of the system to an alternating driving force. In particular we calculate the size of the interference steps and show that a mesoscopic junction (either normal or Josephson) can be used as a phase-voltage converting element. Results are presented in a form suitable for comparison with experiment. We suggest specific experiments to verify our predictions.

I. INTRODUCTION

Recent advances in the fabrication of submicron systems[1] have made it possible to study experimentally phenomena on mesoscopic length scales. From the theoretical point of view this is of interest since we are dealing with systems which have many degrees of freedom but are not sufficiently large to be in the thermodynamic limit. Yet despite these degrees of freedom, the systems are small enough to demonstrate quantum-mechanical dynamics and coherence such as those found in microscopic systems.[2] In addition, since we are specifically interested in systems that are coupled to an external driving force, the question of how to describe such open systems within a quantum-mechanical framework naturally arises. From the experimental and technological point of view it is hoped that the study of mesoscopic electronic systems will lead to new applications in logical elements and sensitive measurement devices.

Here we initially focus on the recently predicted voltage oscillations in mesoscopic normal tunnel junctions[3–7] with an ultrasmall capacitance C, when they are driven by an ideal current source, I_{dc}. Various models predict that the application of a current source to such junctions will produce voltage oscillations with an amplitude of $e/2C$, and a frequency I_{dc}/e, similar to the predicted Bloch oscillations of frequency $I_{dc}/2e$ in ultrasmall capacitance Josephson junctions.[8–10] There are several requirements for the observability of this "inverse Josephson effect" in normal (i.e., not superconducting) junctions, many of which will be detailed here. One requirement is a large single electron-charging energy. With current technology junctions with a capacitance $\approx 10^{-17}$ F can be produced, which implies a charging energy of $e^2/2C \approx 100$ K.

In Sec. II we review the semiclassical description of noncoherent Bloch oscillations in normal tunnel junctions.[5–7] In this approach the time evolution of the voltage across the junction is analyzed as a semiclassical stochastic process. The transition rates of electrons tunneling across the junction are calculated assuming that the electrons tunnel independently and elastically. The effect of the small capacitance is accounted for by shifting the relative Fermi energy of the two sides of the junction by $e^2/2C$ once an electron transfer takes place. The net result of this shift is to suppress tunneling if the biasing voltage is smaller than $V_C = e/2C$. When the external voltage exceeds V_C the current source continues to charge the junction, until an electron tunnels and lowers the voltage by e/C. This repeated cycle of continuous uniform charging and stochastic discharging gives rise to a sawtooth voltage. Long time correlations in these sawtooth oscillations result in a power spectrum with δ-function peaks. In Sec. II we also present numerical results for the I-V characteristics and power spectra, along with analytic approximations. Many of the results shown here have been previously obtained by Averin and Likharev;[5,6] we present them mainly for comparison with the results of later sections. In addition we discuss some of the implicit assumptions,[7] at present without micro-

scopic justification, that are made in the semiclassical approach. These assumptions were not explicitly stated in earlier derivations.[5,6] Our main new result in this section is the description of the effect of increasing the temperature. We show that in the semiclassical approach increasing the temperature results in a decrease of the average voltage towards the value RI_{dc}; in the coherent model the effect of temperature is quite different.

In Sec. III we discuss a coherent model for a system whose instantaneous energy as a function of the total charge pushed into the system by an external source is similar to the "nearly free electron" model in the "extended-Brillouin-zone" picture.[11] Such a structure of energy bands is obtained from a quantum-mechanical treatment of the Hamiltonian assumed for the system. An instantaneous state of the system may be described as a coherent superposition of eigenstates of the charge operator, hence the term "coherent picture." When such systems are driven by a weak external source they tend to follow the energy levels adiabatically so that the energy of the system and other variables, such as the voltage, are periodic functions of time. However, in such a model the coupling to external degrees of freedom, i.e., the "heat bath" is extremely important. We discuss the relevance of the model to other mesoscopic systems.

In Sec. IV we include the effects of both Zener tunneling and inelastic transitions between the energy bands in the discussion of the coherent model. In our coherent toy model the single degree-of-freedom wave function describing the system "leaks" to higher bands with time. Neglecting interference effects between consecutive Zener transitions,[12,13] which can be done when the phase smearing time is sufficiently short, one can show that the system displays an unphysical drift to arbitrarily high energy bands, while displaying a new "spiky" type of noise.[4,13] However, this picture has to be qualitatively modified when interference effects in the energy-band picture are important.[14] In a more realistic picture in which the system is coupled to a heat bath, we allow for inelastic transitions among the bands. The average drift is now zero, and one can calculate the steady-state dynamics of the junction. For a specific mechanism of inelastic relaxation we find that the resulting dynamics is very similar to that predicted by the semiclassical model.

The effect of an oscillating driving force on both the coherent and noncoherent Bloch oscillations is discussed in Sec. V. It is mentioned in Refs. 3–6 and 10 that when such a system is driven by both alternating and direct currents simultaneously the response shows "inverse Shapiro"-type steps. The steps should be observed at values of $2\pi I_{dc}/e=(n/m)\omega_{ex}$, where ω_{ex} is the frequency of the external driving force and I_{dc} is the external current. In Sec. V we present a numerical and analytical study of these steps, according to the two pictures, as a function of the parameters. Unlike the case of ordinary "Shapiro steps,"[15] in our case the steps are scanned by changing the phase of the oscillating driving force. This effect suggests that the mesoscopic Josephson and normal junctions can be used as phase-voltage converters. We also discuss the response of junctions to an alternating external bias charge.

A brief discussion of our results is presented in Sec. VI, along with possible experiments to test them. In the Appendix we present a discussion of the differences between current and voltage sources in mesoscopic tunnel junctions.

II. NONCOHERENT BLOCH OSCILLATIONS

In this section we discuss the I_{dc}/e oscillations[3–7] in mesoscopic normal tunnel junctions using the semiclassical approach.[5–7] To clarify the presentation we first calculate the resistance of a junction driven by an ideal voltage source V. In this case the average current is given by[16]

$$\langle I\rangle = er(Q) = \int_{-\infty}^{\infty} D(E)\tau^{-1}(E)f(E) \times [1-f(E+eV)]dE \ . \tag{2.1}$$

$r(Q)$ is the rate of electron tunneling in the direction of the applied voltage as a function of Q, the charge across the junction; $D(E)$ is the density of the single electron energy states; $\tau^{-1}(E)$ is the elastic tunneling rate for an electron of energy E through the barrier; f is the equilibrium-Fermi-distribution function

$$f(E)=\frac{1}{\exp(E/k_BT)+1} \ . \tag{2.2}$$

The charge Q is related to the voltage by $Q=CV$. To obtain Eq. (2.1) we made the following assumptions:

(1) The voltage is sufficiently large, that is $eV \gg k_BT$, so that we may neglect the backward transition rate $l(Q)$ relative to $r(Q)$.

(2) The equilibration time in both electrodes is much shorter than the tunneling time $\tau(E)$ so that the occupation probabilities of the states are given by the equilibrium Fermi distribution.

(3) The quantum probabilities for the elastic tunneling of electrons of different states are independent.

(4) After a charge has tunneled across the junction the voltage source, a device with zero internal resistance (see the Appendix), removes it instantaneously so that a fixed voltage is maintained across the junction at all times.

Although we assume that the electrons tunnel elastically there is still dissipation in the junction. For example, the electrons that tunnel from the left-hand side to the right-hand side electrode are not, generally, in thermal equilibrium with those on the right-hand side. As they thermalize they release energy to the heat bath coupled to the system, and generate dissipation at a rate IV.

In the case of a tunnel junction between two metallic electrodes it will be assumed that both $D(E)$ and $\tau^{-1}(E)$ depend only weakly on energy and can be replaced by their value at the Fermi energy, $D(E_F)$, and $\tau^{-1}(E_F)$. Since the integral of the occupation factor $f(1-f)$ is approximately eV, we then have

$$I=e^2\tau^{-1}(E_F)D(E_F)V \ , \tag{2.3}$$

so the resistance is given by

$$R \equiv \frac{1}{e^2\tau^{-1}(E_F)D(E_F)} . \tag{2.4}$$

In a small junction $D(E)$ and $\tau^{-1}(E)$ may have a strong energy dependence, but this is not expected to modify the above discussion qualitatively so long as this dependence is smooth. Note that for the case of quasiparticle tunneling between two superconductors, $D(E)$ diverges on either side of the energy gap. Consequently there is a large increase in the current when the applied voltage exceeds $2\Delta(T)/e$.[17]

We now turn to the case that the junction is driven by an external current source I_{dc}. An ideal current source, by definition, has an infinite internal resistance (see the Appendix). Therefore, an electron that tunnels across the junction changes the voltage by an amount e/C. Consider a junction with an initial voltage drop V. The electron that tunnels elastically across the junction from an energy E relative to the Fermi energy on the left-hand side arrives on the right-hand side not at an energy $E+eV$ (relative to E_F on the right-hand side), but rather at energy $E+eV-e^2/2C$. Including this shift the transition rates are given by

$$r(Q)=\int_{-\infty}^{\infty} D(E)\tau^{-1}(E)f(E) \times[1-f(E+eV-e^2/2C)]dE , \tag{2.5}$$

$$l(Q)=\int_{-\infty}^{\infty} D(E)\tau^{-1}(E)f(E) \times[1-f(E+eV-e^2/2C)]dE ,$$

where again $Q=CV$. Using the definition of the resistance R in Eq. (2.4), it is convenient to express the transition rates as

$$r(Q)=\frac{1}{RC}P_{r,l}(Q), \quad l(Q)=\frac{1}{RC}P_{l,r}(Q) , \tag{2.6}$$

where

$$P_{r,l}=\int_{-\infty}^{\infty} f(E)\left[1-f\left[E+\frac{Q}{e}-\frac{1}{2}\right]\right]dE ,$$
$$P_{l,r}=\int_{-\infty}^{\infty} f(E)\left[1-f\left[E-\frac{Q}{e}+\frac{1}{2}\right]\right]dE , \tag{2.7}$$

and the energy is measured in units of e^2/C.

In the semiclassical approach the state of the system is described by the classical variable Q, the charge across the junction. The time evolution of Q is described by the stochastic process

$$Q(t+\Delta t)=\begin{cases} Q(t)+I_{dc}\,\Delta t+e & \text{with probability } l(Q)\Delta t , \\ Q(t)+I_{dc}\,\Delta t-e & \text{with probability } r(Q)\Delta t , \\ Q(t)+I_{dc}\,\Delta t & \text{with probability } 1-[r(Q)+l(Q)]\Delta t . \end{cases} \tag{2.8}$$

In writing the stochastic process this way we have explicitly assumed that the current source I_{dc} pushes in a continuous charge at a uniform rate while the tunneling of charge occurs discretely, and that Δt is sufficiently small so that at most one charge tunnels during any given time interval. From the stochastic process of Eq. (2.8) we can derive the master equation[18,19]

$$\frac{\partial\rho(Q,t)}{\partial t}=-I_{dc}\frac{\partial\rho(Q,t)}{\partial Q}+r(Q+e)\rho(Q+e,t) +l(Q-e)\rho(Q-e,t) -[r(Q)+l(Q)]\rho(Q,t) . \tag{2.9}$$

This master equation has already been derived in Refs. 5–7. In Refs. 5 and 6 this master equation was derived by considering the dynamics of a quantum density matrix. We emphasize that the assumptions we state here explicitly were implicit in Refs. 5 and 6.

We further discuss the assumptions made in the derivation of Eq. (2.9). In defining the stochastic process in Eq. (2.8) we have assumed that the state of the junction can be described by a single classical degree of freedom Q. The effect of the internal degrees of freedom is expressed by the transition rates $r(Q)$ and $l(Q)$. To clarify this point we work out explicitly the tunneling rates. Let the system be at a state associated with the macroscopic degree of freedom $Q=e/2$ (the charge across the junction is $Q=e/2$.) As we further increase Q by an increment, δQ, the charging energy increases to $(e/2+\delta Q)^2/2C$, which exceeds the energy the system would have if one electron had tunneled by $\sim 2e\,\delta Q/2C$. We stress again that contributions of the tunneling Hamiltonian and the coupling to the heat bath have been neglected in calculating the energy of the system according to this semiclassical picture. From Eqs. (2.6) and (2.7) we calculate $r(e/2+\delta Q)\equiv\bar{r}(\delta Q)$, given by

$$\bar{r}(\delta Q)\approx\begin{cases} \dfrac{k_BT}{e^2R} & \text{if } \delta Q=0 , \\ \dfrac{\delta Q}{eRC} & \text{if } e\,\delta Q/2C \gg k_BT . \end{cases} \tag{2.10}$$

This means that the transition rate increases linearly with δQ for large enough δQ. Energy is conserved in this tunneling process. The charging energy of the system is reduced following the charge transfer, but the electron which tunnels from right to left makes a transition to an

energy level of the left-hand side electrode which is higher than E_F on the left, as mentioned above. Thus the electron gains the change in the charging energy. It is assumed that following its tunneling this "hot" electron relaxes by transferring its excess energy to the heat bath so that the equilibrium Fermi distribution is achieved on either side of the junction. From this discussion one can see that the semiclassical picture includes quite a few phenomenological assumptions and that a genuinely microscopic picture is still lacking.

We now discuss the response of a junction to a direct-current source as described by the stochastic process of Eq. (2.8) assuming that the semiclassical picture is correct. First we consider the limit $k_B T \ll e^2/2C$ so that $r(Q)$ can be approximated by (Fig. 1.)

$$r(Q)=\begin{cases}0, & Q<e/2\ , \\ \dfrac{Q/e-\frac{1}{2}}{RC}, & Q>e/2\ .\end{cases} \tag{2.11}$$

In Fig. 2 we show the I-V characteristics obtained by numerical simulation of the stochastic process described by Eq. (2.8). At low currents ($I_{dc} \ll e/RC$) the voltage traces out a sawtooth wave as a function of time, with $\bar{Q}$ being the average value of Q at which a transition takes place. From Fig. 4 one can see that the average voltage across the junction is related to $\bar{Q}$ by

$$\langle V\rangle=\frac{1}{C}\left[\bar{Q}-\frac{e}{2}\right], \tag{2.12}$$

where Q, the average voltage at which an electron tunnels, is given by

$$\bar{Q}=\int_{-\infty}^{\infty} Q' P(Q') dQ' , \tag{2.13}$$

and $P(Q)$ is the probability density that the transition

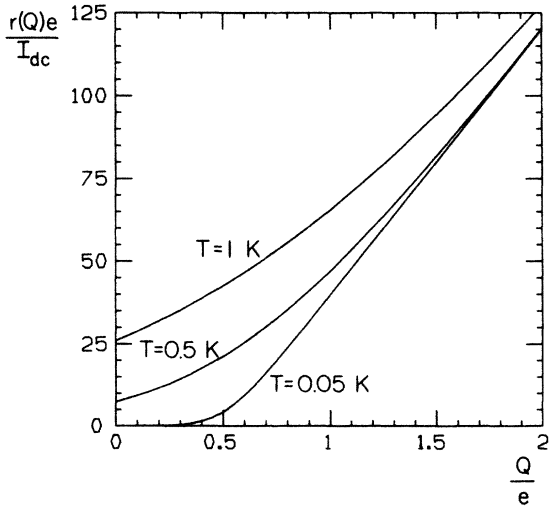

FIG. 1. The transition rate $r(Q)$ vs Q for various values of T. $l(Q)$ is the reflection of $r(Q)$ about the $Q=0$ axis. The parameters are $R=2500\ \Omega$ and $C=1$ fF, so that $e/RC=64$ nA and $I_{dc}=1$ nA.

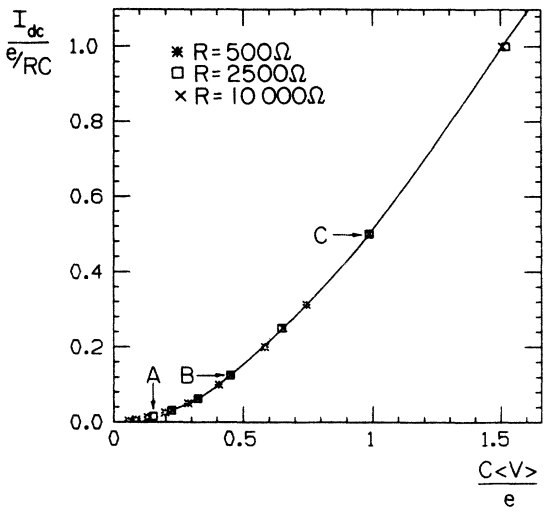

FIG. 2. The I-V characteristic for the semiclassical picture. The parameters are $C=1$ fF and $T=0.05$ K.

occurs when the charge across the junction is Q, namely,

$$P(Q)=\frac{r(Q)}{I_{dc}}\exp\left[-\int_{e/2}^{Q}\frac{r(Q')}{I_{dc}}dQ'\right]. \tag{2.14}$$

This transition probability density is the product of the probability that the junction has *not* made a transition up to the charge Q, times the probability of a transition occurring at Q (Fig. 3).

Using Eq. (2.14) together with Eq. (2.11) we obtain, for $I_{dc} \ll e/RC$,

$$I_{dc}=\frac{2}{\pi}\frac{C}{\mathrm{Re}}\langle V\rangle^2 \tag{2.15}$$

in agreement with the numerical simulations shown in Fig. 2. It can be seen that the I-V characteristic changes

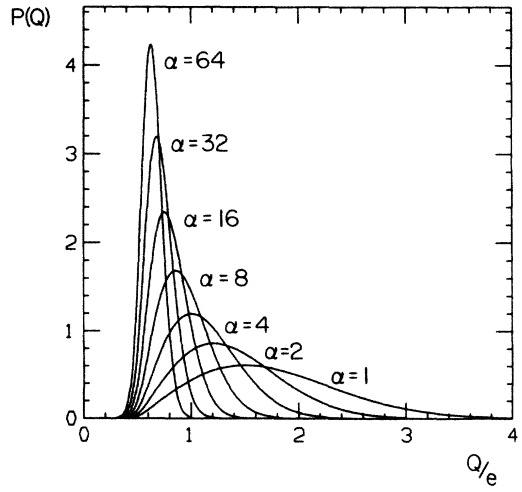

FIG. 3. The dependence of the probability $P(Q)$ on the ratio $\alpha=(e/RC)/I_{dc}$. The width of the distribution varies inversely with α.

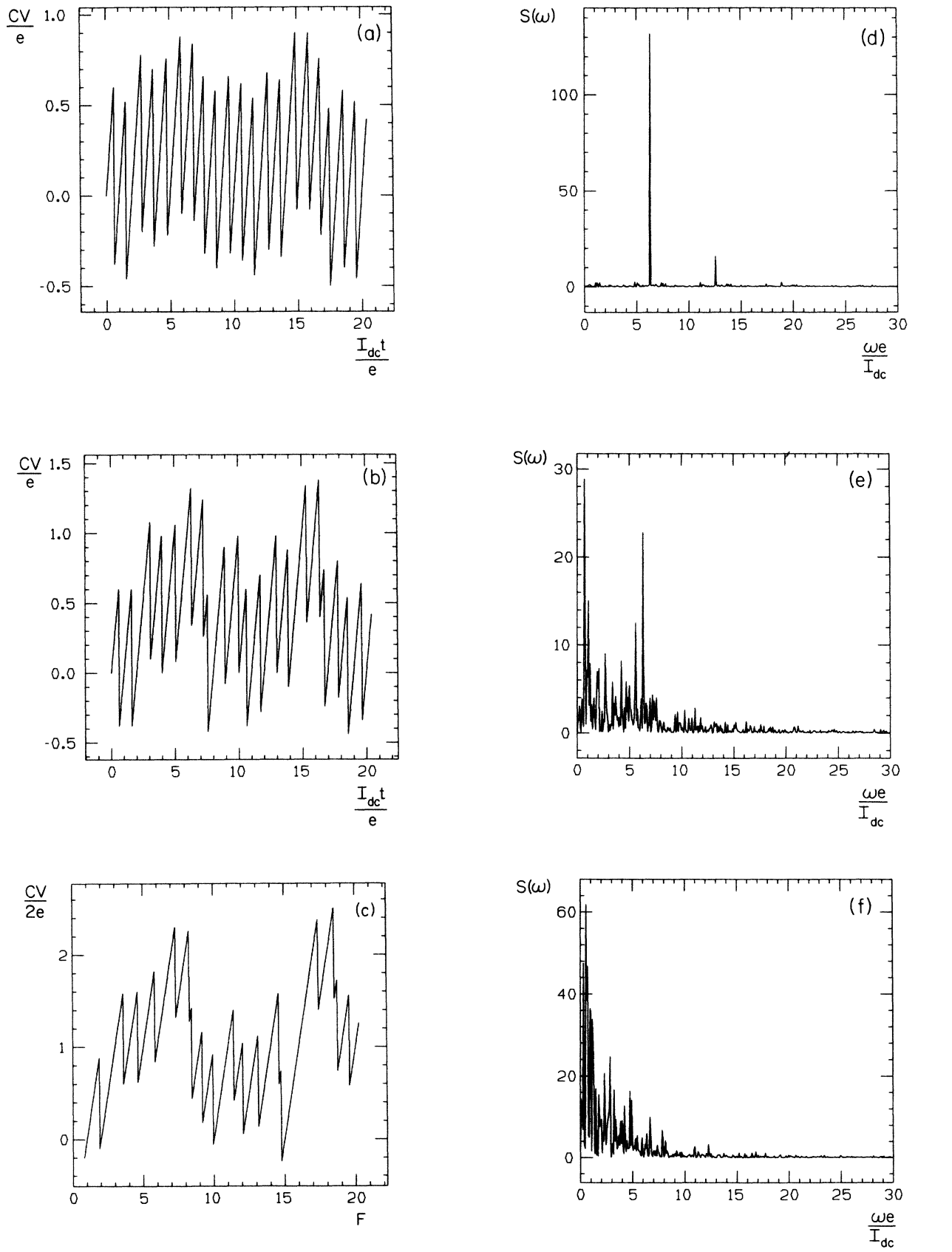

FIG. 4. $V(t)$ as calculated numerically from Eq. (2.8). Processes (a), (b), and (c) correspond to the points A, B, and C in Fig. 2, and (d), (e), and (f) are the corresponding power spectra. Note the difference in the background noise between these power spectra and those of Fig. 3 of Ref. 10. ($F = I_{dc}t/e$).

(approaches linearity) at high currents ($I_{dc} > e/RC$) when the average voltage is greater than e/C. In deriving Eq. (2.15) we have assumed that $\langle V \rangle < e/C$, so that after a transition the voltage across the junction becomes negative. For this reason the lower limit of integration in Eq. (2.14) was taken to be $e/2$. At high currents we can correct Eq. (2.14) and calculate the average voltage using $C\langle V \rangle - e/2$ as the lower limit in the integral. However, we can use a simpler approximate method by setting $\langle Q \rangle = C\langle V \rangle$, and by noting that at each transition Q decreases by exactly e. Therefore, when the junction reaches a steady state, the integral of the transition rate over time must equal the amount of charge pushed in by the current source. In the time interval it takes to bring in one charge we have

$$\int_{\langle Q \rangle - e/2}^{\langle Q \rangle + e/2} \frac{r(Q)}{I_{dc}} dQ = 1 , \tag{2.16}$$

which yields

$$\langle V \rangle = \frac{\langle Q \rangle}{C} = RI_{dc} + \frac{e}{2C} . \tag{2.17}$$

Equation (2.16) is valid when the width of $P(Q)$ is much larger than e. Equation (2.17) is in agreement with the results of the numerical simulations shown in Fig. 2, as well as those of Refs. 5 and 6. As can be seen in Fig. 2, the I-V characteristic scales with $I_{dc}RC$. To understand this behavior and the shape of the I-V characteristics we have plotted the transition probability density $P(Q)$ (Fig. 3). We note that the width of the distribution is proportional to $I_{dc}RC$. We also mention that, since the I_{dc}/e oscillations are due to the discrete transfer of single electrons, to observe these oscillations the width of the distribution must be smaller than e. This corresponds to $I_{dc} \ll e/RC$, the limit we mentioned above.

In Fig. 4 we show the time dependence of the stochastic process for different values of the current and the corresponding power spectra. At low currents we can observe the oscillations at a frequency I_{dc}/e. In this limit the background noise in the power spectrum is in accordance with Refs. 20 and 21. Here we are interested in S_V, the spectral density of the voltage fluctuations. To employ the results of Refs. 20 and 21 we have to view the tunnel junction as an RC circuit. Then $S_V = |Z|^2 S_I$, where S_I is the power spectrum of the current noise and $|Z|^2 = R^2/(1+\omega^2 C^2 R^2)$. The I_{dc}/e oscillations appear in the power spectrum as peaks of zero width at angular frequencies $\omega = 2\pi l I_{dc}/e$, where l is an integer.

As the current increases the background shot noise also increases, so that when $I_{dc} \gg e/RC$ the width of $P(Q)$ is much larger than e and the oscillations are washed out by the noise. In this limit the power spectrum of the current noise approaches that of "classical" shot noise, $S_I \approx eI_{dc}$. Therefore the power spectrum of S_V has high contributions at low frequencies as shown in Fig. 4.

The sharpness of the peaks can be explained as follows. Let $\rho(Q_1,t_1;Q_2t_2)$ be the conditional probability density that the charge on the junction at time t_2 is Q_2 given that at time t_1 the charge on the junction was Q_1. This we will write as $\rho(Q_2,t_2)$ for short. The master equation (2.9), with the initial condition

$$\lim_{t \to t_1} \rho(Q,t) = \delta(Q - Q_1) , \tag{2.18}$$

has a periodic solution $\rho_P(Q,t)$,[5,6] to which the solution $\rho(Q_1,t_1;Q,t)$ of Eqs. (2.9) and (2.18) converges as $t \to \infty$. Thus

$$\rho(Q_1,t_1;Q,t) = \rho_D(Q_1,t_1;Q,t) + \rho_P(Q,t) , \tag{2.19}$$

where $\rho_D(Q_1,t_1;Q,t) \to 0$ as $t \to \infty$. Using the Markov property of the stochastic process $Q(t)$, we can write

$$\begin{aligned} \text{Prob}\{Q(t)=Q_1, Q(t+\tau)=Q_2 \mid Q(0)=Q_0\} &= \text{Prob}\{Q(t+\tau)=Q_2 \mid Q(t)=Q_1\} \times \text{Prob}\{Q(t)=Q_1 \mid Q(0)=Q_0\} \\ &= \rho(Q_1,t;Q_2,t+\tau)\rho(Q_0,0;Q_1,t) , \end{aligned} \tag{2.20}$$

where $\rho = \rho_D + \rho_P$, as in Eq. (2.19). Turning to the autocorrelation function $A(t_1,t_2)$ we have that

$$A(t,t+\tau) = \int\int Q_1 Q_2 \text{Prob}\{Q(t)=Q_1, Q(t+\tau)=Q_2 \mid Q(0)=Q_0\} dQ_1 dQ_2 . \tag{2.21}$$

Using Eqs. (2.19) and (2.20) in Eq. (2.21) and letting $t \to \infty$ along a sequence of periods we obtain

$$A(t,t+\tau) = \int\int Q_1 Q_2 \rho_P(Q,t)[\rho_D(Q_1,0,Q_2,\tau) + \rho_P(Q_2,\tau)] dQ_1 dQ_2 . \tag{2.22}$$

Thus the autocorrelation function

$$A(t) = \lim_{t \to \infty} A(t,t+\tau) \tag{2.23}$$

is a sum of a periodic function and a decaying function of τ. This accounts for the sharp peaks and for the background in the power spectrum. In simple terms this means that the current source serves as an external clock. Tunneling events are highly correlated; they have a stationary distribution about a fixed-time periodic sequence of period e/I_{dc}. As we will show below, the coherent approach yields similar peaks.

III. COHERENT BLOCH OSCILLATIONS

In this section we consider a model system whose energy spectrum as a function of an external driving force F is analogous to that obtained in the extended-zone scheme. With both mesoscopic Josephson junctions and one-dimensional metal rings in mind we assume the system is

described by the Hamiltonian

$$H=E_k(F-\hat{n})^2+H_T \ . \tag{3.1}$$

The first term in Eq. (3.1) is the "kinetic energy," whereas the second term plays the role of a "potential energy." In the case of *current-driven mesoscopic Josephson junctions*[8-10] the driving term is $F=I_{dc}t/2e$ (only Cooper-pair current is considered at this point), and $E_k=2e^2/C$, where C is the capacitance of the junction. The number operator which counts the number of Cooper pairs that have been transferred across the junction is $\hat{n}=-i\partial/\partial\theta$, where θ is the difference in the phase of the macroscopic wave functions on both sides of the junction. Here we shall first consider a case (case I) where H_T is a tunneling Hamiltonian which describes the transfer of a single Cooper pair:

$$\langle n \mid H_T \mid n' \rangle = \tfrac{1}{2}E_T(2\delta_{n,n'}-\delta_{n,n'+1}-\delta_{n,n'-1}) \ . \tag{3.2}$$

In terms of θ,

$$H_T=E_T(1-\cos\theta) \quad \text{(case I)} \ , \tag{3.3a}$$

where $E_T=E_J=\hbar I_J/2e$, and I_J is the critical Josephson current. We also consider an opposite limit in which the matrix elements of H_T are independent of $n-n'$ (≥ 1) (case II), so that

$$H_T=E_T\left[1-\sum_{n=0}^{\infty}\cos(m\theta)\right] \quad \text{(case II)} \ . \tag{3.3b}$$

We are interested in calculating the response of the system, defined as

$$V=\frac{1}{2e}\frac{\partial\langle E\rangle}{\partial F} \ . \tag{3.4}$$

In the case of a Josephson junction, V is the instantaneous voltage.

Note that this toy model ignores important ingredients (quasiparticle current, dissipation) needed for a satisfactory comparison with experiment. This present model is discussed here in order to study some conceptually important aspects of the coherent picture.

The Hamiltonian Eq. (3.1) is formally identical to the one employed for *mesoscopic one-dimensional normal-metal rings driven by a time-dependent flux.*[2,14] We consider an electron in a ring of radius R_0, and make the following identifications: $\hat{n}=-i\partial/\partial\theta$, where θ is the polar coordinate, $E_k=\hbar^2/2mR_0^2$, with m being the effective electron mass, $F=\phi/\phi_0$, with $\phi_0=h/e$ being the flux quantum, and ϕ is the externally applied magnetic flux. A linearly increasing flux is the analog of a direct-current source in the Josephson-junction case above. H_T is the potential $V(\theta)$ which connects momentum states that differ by $\Delta k=l/R_0$ where l is an integer. In this case one is interested in the current response of the system to the constant induced electromotive force.

In the absence of H_T the adiabatic energy spectrum consists of a set of parabolas centered at integer values of F as shown in Fig. 5(a) (for $E_T \ll E_k$). Each parabola describes the energy of the system as a function of F for a different eigenvalue of $\hat{n}$. In the coherent picture the inclusion of H_T removes the degeneracies at the points of intersection of the parabolas, producing the energy-band picture shown in Fig. 5(b). For example, consider the specific case of $F=\frac{1}{2}$ at the intersection of the parabolas corresponding to the states $n=0$ and $n=1$. In the absence of H_T the states $|0\rangle$ and $|1\rangle$ (eigenstates of $\hat{n}$) have the same energy, $E_k/4$. It is possible to "build" the symmetric and antisymmetric superpositions

$$\psi_+=\frac{1}{\sqrt{2}}(|0\rangle+|1\rangle), \quad \psi_-=\frac{1}{\sqrt{2}}(|0\rangle-|1\rangle) \ . \tag{3.5}$$

To first order in perturbation theory the corresponding energies are

$$\begin{aligned} E_+ &= \langle\psi_+ \mid H \mid \psi_+\rangle = E_k/4+E_T/2 \ , \\ E_- &= \langle\psi_- \mid H \mid \psi_-\rangle = E_k/4-3E_T/2 \ . \end{aligned} \tag{3.6}$$

This means that if we prepare the system in the $n=0$ or $n=1$ state it will oscillate coherently between these two states with a frequency $\omega=E_T/\hbar$ in a fashion similar to

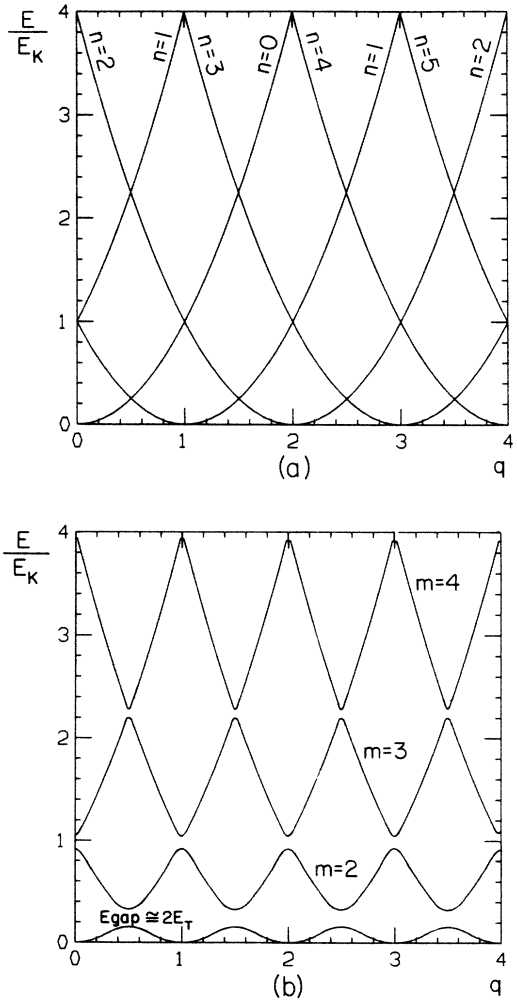

FIG. 5. The energy spectrum of the Hamiltonian (3.1): (a) in the absence of H_T; (b) the band structure when H_T is included as a perturbation. The energy is measured relative to E_T.

the quantum oscillations of a particle in a symmetric double well.[22–28] The assumption of the existence of these quantum coherent states is the rationale for the name "coherent picture," in contrast to the incoherent transitions in the semiclassical approach.

Including a coupling to a heat bath in our description may renormalize the energy gaps.[29] This is pertinent to the question of whether by biasing the system to a $Q=e/2$ state one will be able to see coherent oscillations between the n states ($|0\rangle$ and $|1\rangle$, for example), similar to the discussions of macroscopic quantum coherence (MQC) in a two-level system[22–28] and experiments that have been suggested to measure MQC in superconducting quantum interference devices (SQUID's).[30] We shall not dwell upon this point but will proceed with the analysis of other aspects of our simple coherent-oscillation model.

For our energy-band picture the response of the system is given by Eq. (3.4); V is periodic in F with period 1. If the system is in the lowest energy band, the amplitude of V, denoted by V_0, is given by

$$V_0 \approx \frac{E_k}{2e}\left[1-\frac{3}{2^{1/3}}(E_T/E_k)^{2/3}+O((E_T/E_k)^{4/3})\right] . \quad (3.7)$$

In Fig. 6 we show $V(F)$ for various different values of E_T/E_k. When $E_T \ll E_k$ the response of the junction has a sawtooth waveform. As E_T increases the voltage becomes more rounded, with amplitude V_0.

IV. THE EFFECT OF ZENER AND INELASTIC TRANSITIONS BETWEEN ENERGY BANDS

When F is varied linearly in time, in principle one has to solve the time-dependent Schrödinger equation. To go beyond the adiabatic approximation we have to take into account the possibility of Zener tunneling among the energy bands. When the system sweeps through a narrow gap region in the energy-time space, the wave function leaks into the neighboring bands. The result is that the wave function eventually spreads toward higher bands at a rate that depends on $\dot{F}$, leading to an increase in the average energy. Physically this means that the external driving force pumps energy into the system. In the absence of inelastic effects this process is reversible and as was pointed out by Landauer,[31] the energy that was pumped into the system is, in principle, retrievable. Interference of different paths in the energy-time space leads to interesting effects, including possibly localization in the energy direction.[14] Any coupling to a heat bath introduces phase randomization and destroys the reversibility of the process on a certain time scale, τ_ϕ. Here we shall consider a case where the phase is completely randomized over a time shorter than half the period of the oscillations, but τ_ϕ is still sufficiently large so that the standard expressions for Zener tunneling through the narrow energy gaps apply. For our model system this implies $\tau_\phi < I_{dc}/e$. One may then neglect interference effects between consecutive Zener events and describe the dynamics of the system in terms of a master equation, accounting for Zener tunneling probabilities (rather than the probability amplitudes). The probability for such a Zener transition from the mth to the $(m+1)$-th band is given by[12,32–34]

$$P_{m,m+1}=P_{m+1,m}=\exp\left[\frac{-\pi}{4}\frac{E_{\rm gap}(m)}{\hbar\Omega(m)}\right] . \quad (4.1)$$

where $E_{\rm gap}(m)$ is the energy gap between bands m and $m+1$. The frequency $\Omega(m)$ is inversely proportional to the time it takes the external driving force to transfer an energy $E_{\rm gap}(m)$ to the system, that is,

$$\Omega(m)=\frac{\dot{F}mE_k}{E_{\rm gap}(m)} . \quad (4.2)$$

The Zener probability, Eq. (4.1), is a good approximation for both the adiabatic limit $[\hbar\Omega(m) \ll E_{\rm gap}(m)]$ and the sudden approximation limit $[\hbar\Omega(m) \gg E_{\rm gap}(m)]$. We define the "Zener time" τ_Z as the time it takes for the system to develop half of $p_{m,m+1}$ as it travels through the narrow gap region. This time is proportional to $\Omega^{-1}(m)$ in the adiabatic limit,[33] so that our analysis is valid for

$$\dot{F} < \tau_\phi^{-1} < \dot{F}\left[\frac{mE_k}{E_{\rm gap}(m)}\right] . \quad (4.3)$$

When $\tau_\phi \lesssim \tau_Z$ we have to take into account the corrections of the Zener probability due to the effect of the heat bath.[34]

It is easier to understand the effect of the Zener transitions if we first study the dynamics of the system while neglecting the inelastic transitions between the bands. When Eq. (4.3) is valid the time evolution of the system can be treated as a stochastic process involving two variables: the band number m and a "spin" s which is defined as the sign of $\partial E/\partial F$, so that s may assume the values ± 1. The stochastic process can be treated as a discrete random walk in which the time step is $1/2\dot{F}$. If at time step i the system is in band $m(i)$ with spin $s(i)$, then the stochastic process is defined as

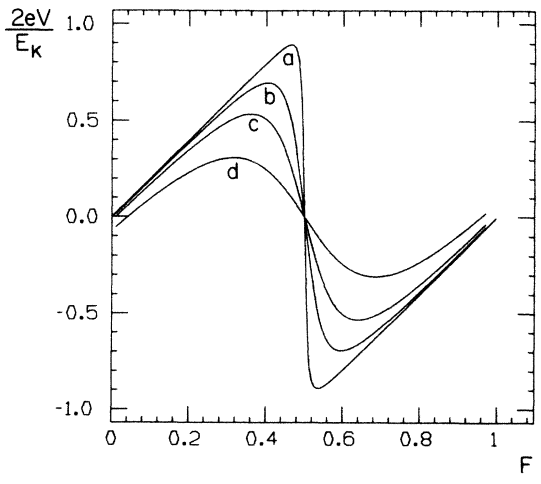

FIG. 6. $V(F)$ according to the coherent picture. The parameters are (a) $E_T/E_k=0.01$, (b) $E_T/E_k=0.05$, (c) $E_T/E_k=0.10$, and (d) $E_T/E_k=0.20$.

$$m(i+1)=m(i) \text{ and } s(i+1)=-s(i) \text{ with probability } 1-P_{m,m+s(i)} , \tag{4.4a}$$

and

$$m(i+1)=m(i)+s(i) \text{ and } s(i+1)=s(i) \text{ with probability } P_{m,m+s(i)} , \tag{4.4b}$$

and where all transitions not explicitly listed are forbidden. Since the probability of Zener tunneling increases with band number, at high band numbers, once the system tunnels upward it has a higher probability of continuing upwards rather than staying in a given band. Similarly, at high band numbers, once the system undergoes a transition downward it has a high probability of continuing to move down in band number. Hence we expect to observe long trajectories up and down in band number as shown in Fig. 7(a). These "spiky" trajectories reflect the fact that occasionally the junction charges up to a high voltage and then rapidly discharges. The longer we wait the higher are the spikes we observe. These spikes contribute to the low frequency part of the "power spectrum" as shown in Fig. 7(b). We emphasize that, strictly speaking, we cannot define the power spectrum of the stochastic process described by Eq. (4.4) because the process itself is not stationary; it has an unbounded drift to higher band numbers. This drift is related to the fact that for a given band m, we have that $P_{m,m+1}>P_{m,m-1}$. This drift reflects the fact that the external driving force pumps energy into the system via incoherent Zener transitions.

To study the drift we can write the following master equations that correspond to the stochastic process:

$$\begin{aligned}\rho(m,s=+1,t=n)&=\rho(m-1,s=+1,t=n-1)P_{m-1,m}+\rho(m,s=-1,t=n-1)(1-P_{m,m-1}) ,\\ \rho(m,s=-1,t=n)&=\rho(m+1,s=-1,t=n-1)P_{m+1,m}+\rho(m,s=+1,t=n-1)(1-P_{m,m+1}) .\end{aligned} \tag{4.5}$$

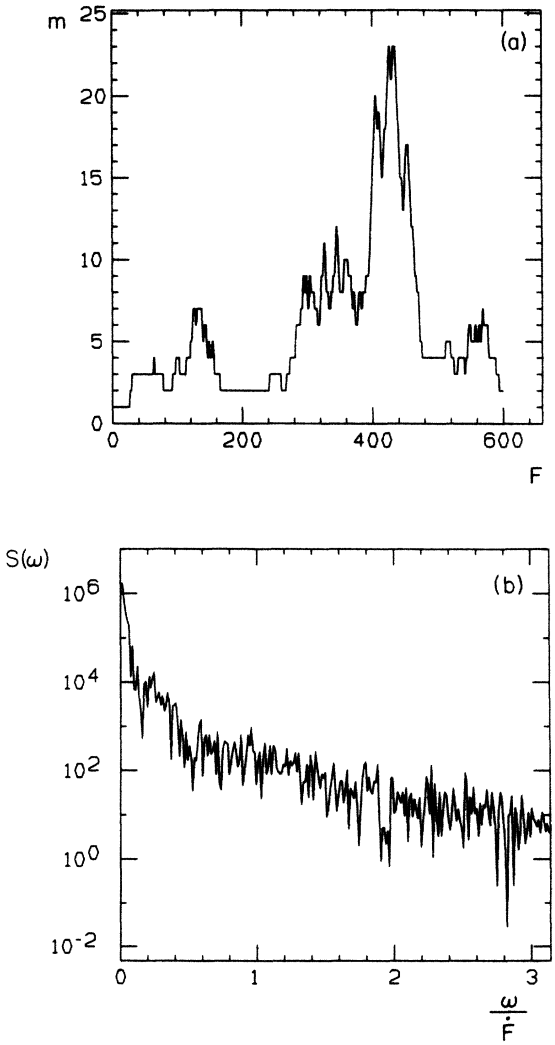

FIG. 7. Results of numerical simulations of the stochastic process of Eq. (4.4), for case II, when $\pi E_{\rm gap}/4\hbar\Omega=8$. (a) The band number m as a function of F. (b) The corresponding power spectrum.

For case II and $\hbar\Omega(m)>E_{\rm gap}(m)$ the drift rapidly becomes linear in time, as shown in Fig. 8. For case I the approach is even more rapid.

Clearly this unbounded drift is not physical. As we continue to pump energy into the system its effective temperature increases. The system can dissipate energy by means of inelastic transitions among the bands, thus balancing the drift. Such downward transitions can occur even when the temperature of the coupled heat bath is zero. At nonzero temperatures there is also the finite probability for the system to absorb a phonon from the bath, thus undergoing a transition upward. However, as long as $k_BT<E_{\rm gap}(m)$, such transitions may be neglected.

In order to facilitate comparison with the semiclassical picture of a normal tunnel junction we next consider a special case of inelastic transitions. We allow only for transitions corresponding to a change of $\Delta F=\pm 1$. This corresponds to the inelastic transfer of a single Cooper pair, in the case of a Josephson junction, or a momentum transfer of $\hbar/R_0$ in the case of the ring. We further assume that the inelastic transition rate $\tau_{\rm in}^{-1}$ is proportional to the energy difference between the initial and final state, ΔE:

$$\tau_{\rm in}^{-1}=\eta\frac{\Delta E}{\hbar} , \tag{4.6}$$

where η is the dimensionless constant measuring the coupling to the heat bath.[22,34] From Fig. 9 it can be seen that ΔE is given by

$$\Delta E(F)=2E_k(F-\tfrac{1}{2}) . \tag{4.7}$$

In analogy with the analysis of the semiclassical model we define an inelastic resistance

$$R_{\rm in}=\frac{\hbar}{e^2}\frac{1}{\eta} . \tag{4.8}$$

To include the inelastic transitions the discrete-time stochastic process of Eq. (4.4) (the Zener transitions) is superimposed on a continuous-time stochastic process to obtain

$$\begin{bmatrix} m(t+\Delta t) \\ s(t+\Delta t) \end{bmatrix} = \begin{cases} \begin{bmatrix} m(t) \\ -s(t) \end{bmatrix} & \text{with probability } 1-P_{m,m+s(t)} \text{ if } t<n/2<t+\Delta t \ , & (4.9a) \\ \begin{bmatrix} m(t)+s(t) \\ s(t) \end{bmatrix} & \text{with probability } P_{m,m+s(t)} \text{ if } t<n/2<t+\Delta t \ , & (4.9b) \\ \begin{bmatrix} m(t)-2 \\ s(t) \end{bmatrix} & \text{with probability } \tau_{\text{in}}^{-1}\Delta t \text{ if } \Delta t \le |t-n/2| \text{ and if } m(t)>2 \ , & (4.9c) \\ \begin{bmatrix} 1 \\ -s(t) \end{bmatrix} & \text{with probability } \tau_{\text{in}}^{-1}\Delta t \text{ if } \Delta t \le |t-n/2| \text{ and if } m(t)=2 \ , & (4.9d) \\ \begin{bmatrix} m(t) \\ s(t) \end{bmatrix} & \text{with probability } 1-\tau_{\text{in}}^{-1}\Delta t \text{ if } \Delta t \le |t-n/2| \text{ and if } m(t)<2 \ , & (4.9e) \end{cases}$$

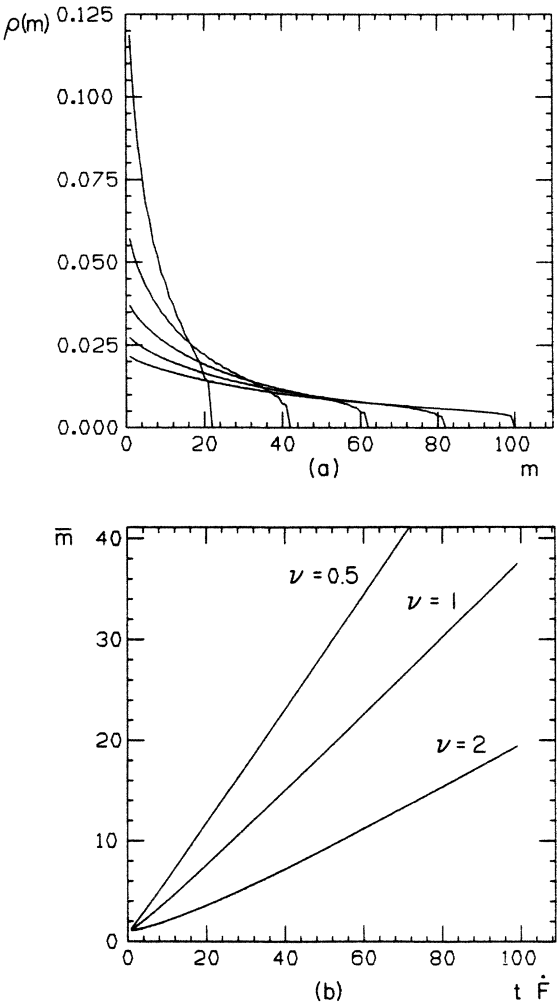

FIG. 8. The time evolution of the probability density $\rho(m)$ as calculated from the master equation given in Eq. (4.5) for case II, showing the constant drift upwards in band number. Time is measured in units of $\dot{F}^{-1}$, and $\nu \equiv \pi E_{\text{gap}}/4\hbar\Omega = 1$. (a) $\rho(m)$ at successive times, 10–50 in steps of 10. At $t=0$ the distribution is a δ function at $m=1$. (b) $\bar{m} \equiv \int m\rho(m)dm$ as a function of time for different values of ν.

where again all transitions not listed are forbidden. The master equation given in Eq. 4.5 is replaced by an appropriate master equation[17] that corresponds to Eq. (4.9).

In Fig. 10 we show typical results of the time evolution of $\rho(m)$ calculated from a discrete time approximation to the master equation that corresponds to Eq. (4.9). We see that after a transient time the probability density $\rho(m)$ settles around some average m and the upward drift ceases. In Fig. 11 we show the dc response of the system in the limit $E_{\text{gap}} \to 0$ (the Zener tunneling probability goes to unity). In Fig. 12 the power spectrum of the stochastic process for various values of the driving force is shown. The dependence of $\tau_{\text{in}}^{-1}(F)$ on F has the same functional form as that of $r(Q)$ discussed in Sec. II in the limit of zero temperature. Therefore we can directly apply the results of Sec. II and obtain that the voltage of the system

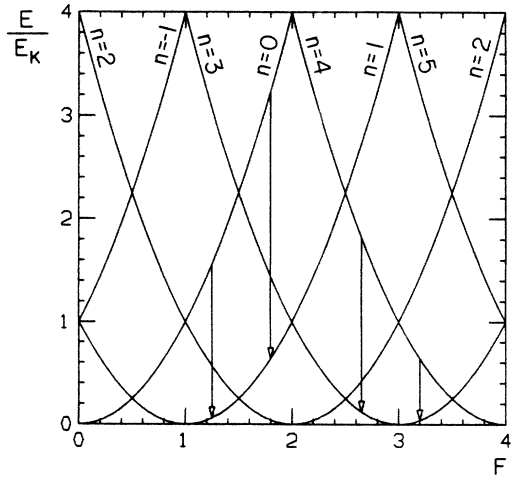

FIG. 9. Description of the inelastic transitions between the energy bands. The arrows are examples of the type of possible transitions used in the stochastic process.

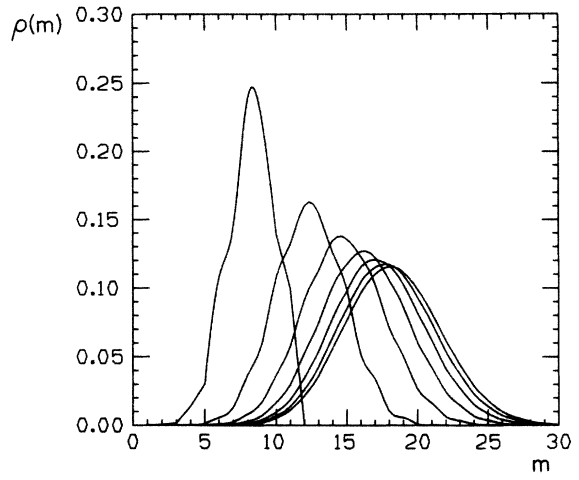

FIG. 10. The time evolution of the probability density $\rho(m)$ as calculated by the master equation for case II when the inelastic transitions are included, and where at $t=0$ the distribution is a δ function at $m=1$. The inelastic transitions compete with the drift observed in Fig. 7, and the two processes balance each other. The parameters are $E_k=1.3\times10^{-4}$ eV, $R_{\rm in}=10^5\ \Omega$, and $\pi E_{\rm gap}=2.8\hbar\Omega$ (case II). Time is measured in units of $\dot{F}^{-1}$, showing $\rho(m)$ from $t=10$ to $t=40$ in steps of 5.

for $\hbar\dot{F}\gg\eta E_k/2$ is given by

$$V=\frac{1}{2e}\left[\frac{\hbar\dot{F}}{\eta}+E_k\right] \tag{4.10}$$

and

$$V=\frac{1}{e}\left[\frac{\pi\hbar\dot{F}E_k}{2\eta}\right]^{1/2} \tag{4.11}$$

for $\hbar\dot{F}\ll\eta E_k/2$.

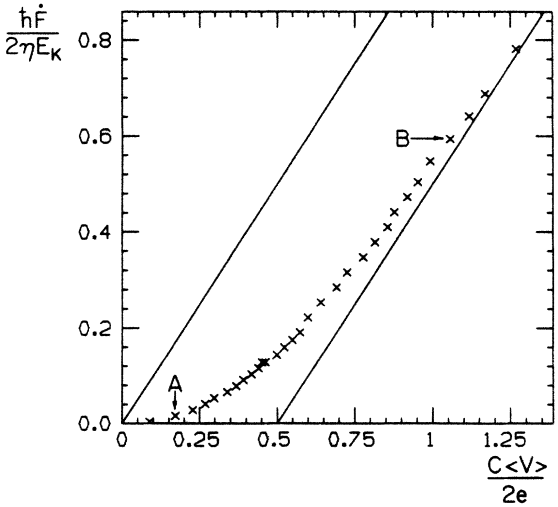

FIG. 11. I-V characteristics calculated numerically by simulating the stochastic process of Eq. (4.10). The parameters are $R_{\rm in}=500\Omega$, $E_{\rm gap}/\hbar\Omega=0$.

We now examine the case of finite Zener probability ($E_{\rm gap}>0$). First we consider the limit $\hbar\dot{F}\ll\eta E_k/2$. In this limit the system stays only on the first and second energy bands; when it undergoes a Zener transition to the second band it relaxes inelastically to the lowest band before undergoing the next Zener transition. The voltage of the system with both inelastic and Zener transitions can be approximated considering these two processes independently; it is equal to the result of the $E_{\rm gap}=0$ case multiplied by the Zener probability. This leads to exponentially small V at low $\dot{F}$. At high currents the system stays at the higher energy bands and the voltage asymptotically approaches that of Eq. (4.10) (case I). In case II the voltage at large $\dot{F}$ is lower than that of case I by an amount proportional to $E_T^2/2eE_k$. In Fig. 13 we show a typical calculated response, the stochastic process and its power spectrum are shown in Fig. 14.

In Sec. III we have examined the relation of the model system to a simplified picture of a mesoscopic Josephson junction. In a real Josephson junction the inelastic transitions are due to quasiparticle tunneling that corresponds to a change of n by $\frac{1}{2}$, as discussed elsewhere.[6,17,35] In such a description one should account for the energy dependence of the quasiparticle density of states. Important ingredients of the above discussions should also be included in the study of mesoscopic normal tunnel junctions.[14,17,36]

V. THE EFFECT OF AN ALTERNATING DRIVING FORCE

We now study the dynamics in the presence of an alternating driving force. In this section we examine the response of mesoscopic systems within both the coherent picture (Sec. III and IV) and the semiclassical picture.

One important effect is the hysteresis in the voltage of the model discussed in Sec. III when the driving force $\dot{F}$ is cycled up and down at a finite rate. In Sec. IV we have argued that for small $\dot{F}$ the system follows nondissipatively the lowest energy band. Zener transitions will occur over a time scale

$$\tau=\frac{1}{\dot{F}}\exp\left[\frac{-\pi}{4}\frac{E_{\rm gap}(1)}{\hbar\Omega(1)}\right]. \tag{5.1}$$

When η is small (the inelastic rate is small), then once the system Zener tunnels to the second band it will tend to continue to climb to higher and higher energy bands. Therefore, to observe large hysteresis, we want $\tau(\dot{F}_{\rm max})$ to be of the order of the inverse frequency of the driving force, where $\dot{F}_{\rm max}$ is the maximum value of $\dot{F}$ in one cycle. Such hysteretic behavior (for case I) is shown in Fig. 15.

We next study the behavior in the presence of both a direct and alternating driving force; that is,

$$F(t)=f_{\rm dc}t-\frac{f_{\rm ac}}{\omega_{\rm ex}}\cos(\omega_{\rm ex}t+\phi)+\frac{f_{\rm ac}}{\omega_{\rm ex}}\cos\phi \tag{5.2}$$

so that

$$f\equiv\dot{F}(t)=f_{\rm dc}+f_{\rm ac}\sin(\omega_{\rm ex}t+\phi)\ , \tag{5.3}$$

where we assumed that $F=0$ at $t=0$. Drawing an analogy with the behavior of macroscopic Josephson junctions driven by microwaves,[37] we expect to observe resonance phenomena when ω_{ex} is commensurate with the angular frequency of the Bloch oscillations. That is, we expect to see "inverse Shapiro" steps in the response of the system when

$$2\pi f_{dc}=\frac{l}{m}\omega_{ex} , \tag{5.4}$$

where l and m are integers. This effect, proposed in Refs. 5–7, is shown schematically in Fig. 16(a). These steps are different than the standard Shapiro steps which are shown in Fig. 16(b). In the latter the steps correspond to regions where the voltage across the junction does not change with the current, so that the step is scanned by varying the current. In systems that exhibit Bloch oscillations the steps should be scanned by holding the amplitudes of the direct and alternating driving force fixed while changing ϕ, the *phase* of the alternating force. To demonstrate this we show in Fig. 17(a) the results of numerical calculations of the average voltage of a normal tunnel junction (semiclassical picture) as a function of ω_{ex}, in the presence of an external current. The average voltage was calculated by numerical simulations of the stochastic process [Eq. (2.8)] replacing I_{dc} by

$$I=I_{dc}+I_{ac}\sin(\omega_{ex}t+\phi) . \tag{5.5}$$

In Fig. 17(b) we show the maximal width of the steps when ϕ is swept from 0 to 2π for selected values of I_{dc}. The first harmonic step ($l=m=1$) is the largest, and the size of the higher harmonic steps becomes smaller, as in the case of Shapiro steps. Since the average voltage changes as a function of ϕ we can use the junction as a phase-voltage converter with maximum sensitivity when $\omega_{ex}=2\pi I_{dc}/e$.

Before proceeding we note that mathematically the

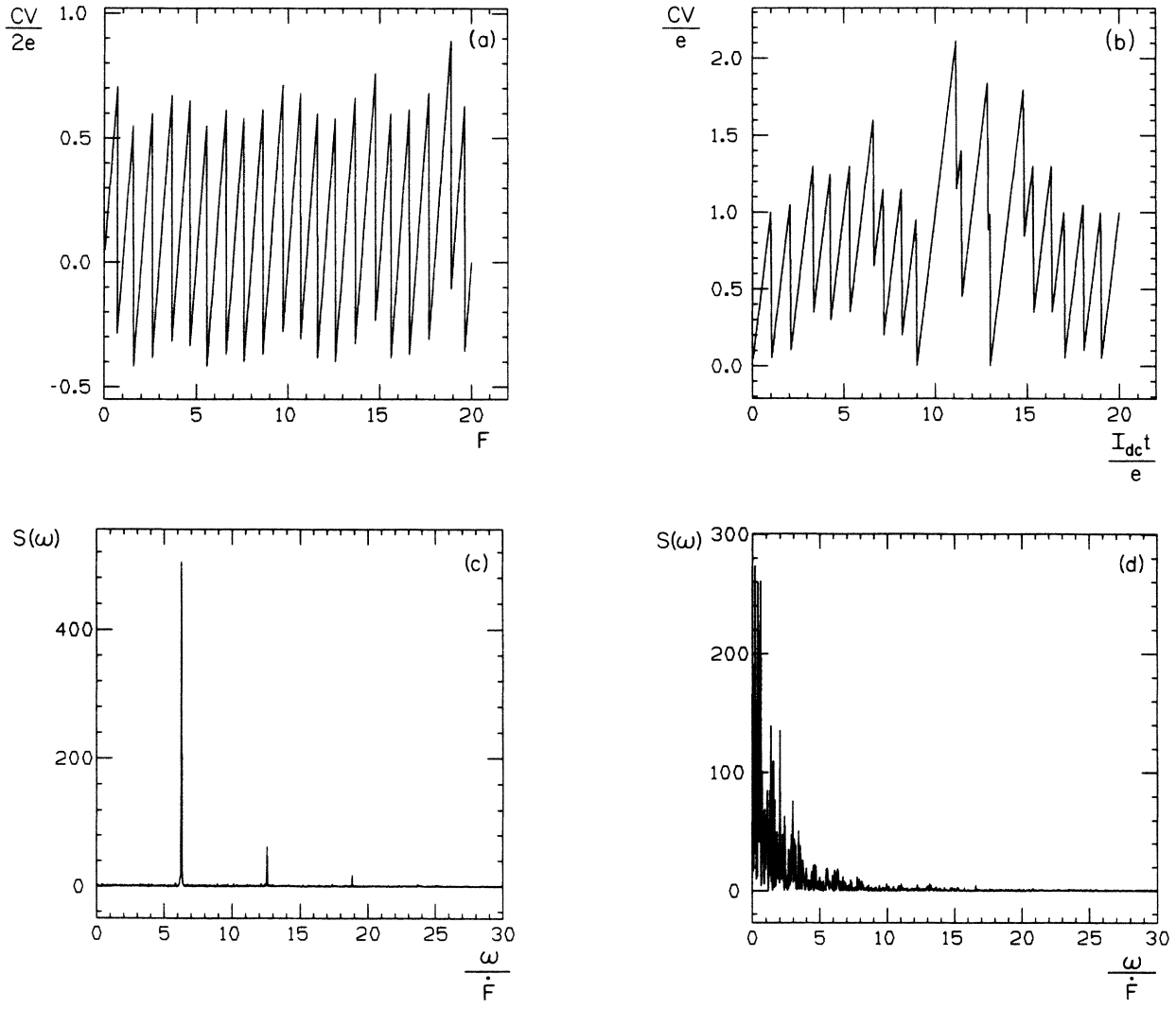

FIG. 12. The stochastic process of Eq. (4.9). Plots (a) and (b) are of $V(t)$ for points A and B in Fig. 11, and (c) and (d) are their corresponding power spectra.

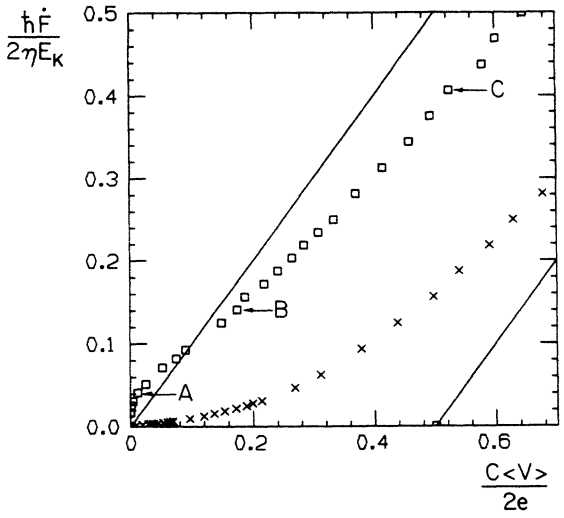

FIG. 13. I-V characteristics for finite Zener tunneling probability calculated numerically by solving the stochastic process of Eq. (4.9). The parameters are $R_{in}=500\ \Omega$, $C=1$ fF, and $\pi E_{gap}^2/4\hbar E_k=25\times10^{10}$ Hz (upper curve) and $\pi E_{gap}^2/4\hbar E_k=0.625\times10^{10}$ Hz (lower curve).

semiclassical picture in the limit of zero temperature and the band picture in the limit $E_{gap}\to0$ lead to the same stochastic process, when the inelastic transitions in the latter are of the form described in Sec. IV. We also note that both approaches in the limit of very short relaxation times yield the same results as the band picture in the limit $P_{0,1}\to0$. To ease the presentation and comparison of the semiclassical and band pictures, we present the following mapping between the parameters of the latter (on the left) and those of the former:

$$f_{dc}\leftrightarrow I_{dc},\quad f_{ac}\leftrightarrow I_{ac},\quad 2e\leftrightarrow e\ ,$$
$$E_k\leftrightarrow\frac{e^2}{2C},\quad V\leftrightarrow V,\quad R_{in}=\frac{\hbar}{e^2}\frac{1}{\eta}\leftrightarrow R\ . \tag{5.6}$$

To demonstrate the possible application of the junction as a phase-voltage converter we present in Fig. 18 the average voltage of the first harmonic step as a function of ϕ. The amplitude of the voltage, that is, the size of the first harmonic step, ΔV_1, depends upon I_{dc}/I_{ac} as shown in Fig. 19. This dependence is again very similar to that in the case of "Shapiro steps."

We turn now to the analytical approximations of the average voltage. First we consider the coherent model in the limit $P_{0,1}\to0$ and $E_T\lesssim E_k$. Under these conditions the system follows the lowest energy band with

$$V(t)\approx V_0\sin[2\pi F(t)]\ , \tag{5.7}$$

where the energy band is approximated by its first harmonic. Here

$$V_0\approx\frac{E_k}{2e}\left[1-\frac{3}{2^{1/3}}(E_T/E_k)^{2/3}+O((E_T/E_k)^{4/3})\right]\ , \tag{5.8}$$

and $F(t)$ is given by Eq. (5.2). The average voltage $\langle V\rangle$ is then calculated by

$$\langle V\rangle=\frac{V_0}{T}\int_0^T\sin[2\pi F(t)]dt\ , \tag{5.9}$$

which can be expressed in terms of Bessel functions. The coherent model (with $E_T\ll E_k$) and the semiclassical picture (with large transition rates) give qualitatively similar results although in the latter the voltage as a function of F is no longer the sinusoidal one of Eq. (5.7) but rather a sawtooth wave. In Fig. 20 we show the effect of temperature on the average voltage of the first harmonic step as a function of I_{ac}/I_{dc}. In the coherent picture, Zener transitions lead to a decrease in step size.

We also study the effect of a bias of the form

$$F(t)=F_0+f_{ac}\sin(\omega_{ex}t+\phi)\ . \tag{5.10}$$

This corresponds to a charge bias with an oscillating component.[35] Within our model of the Josephson junction we define an effective capacitance

$$C_{eff}^{-1}(\omega_{ex})=\frac{\bar V(\omega_{ex})}{2ef_{ac}}\ , \tag{5.11}$$

where $\bar V(\omega_{ex})$ is the sine transform of $V(t)$ as defined below. Here we are mainly interested in the limit of low frequencies. Neglecting Zener tunneling, $\bar V(\omega_{ex})$ can be calculated from $V(t)$ given by Eq. (5.7), and $F(t)$ from Eq. (5.10):

$$\bar V(\omega_{ex})=\frac{\omega_{ex}V_0}{2\pi}\int_0^{2\pi/\omega_{ex}}\sin[2\pi F(t)]\times\sin(\omega_{ex}t+\phi)dt\ . \tag{5.12}$$

This integral can also be expressed in terms of Bessel functions. In Fig. 21 we show C_{eff} as a function of f_{ac}. In Fig. 21 we also show the strong effect of F_0 on $C_{eff}(\omega_{ex})$. The sensitivity of C_{eff} to the bias charge suggests possible applications for detection devices.

An alternative definition of the effective capacitance, offered by Büttiker,[35] is the differential capacitance,

$$C_{eff}'^{-1}=\frac{\partial\langle V\rangle}{\partial Q}=\frac{\partial^2\langle E\rangle}{\partial Q^2}\ . \tag{5.13}$$

This definition draws a strong analogy between the capacitance and an "effective mass" that determines the response of the junction. The definition given in Eq. (5.11) stresses the idea of the capacitor as a dynamic element.

VI. DISCUSSION

In this section we suggest some experiments that may demonstrate the above predictions. The first and simplest experiment is to use the configuration of Fig. 22 in order to induce a static bias charge q (in units of e). Such a configuration has been recently suggested by Büttiker.[35] In the limit $k_BT\ll e^2/2C$ a zero average current is predicted as long as $q<\frac{1}{2}$.[5,6,37,38] One may also study the I-V characteristics of the junction driven by an external dc source I_{dc}. The $e/2C$ shift in the I-V characteristic (Fig. 2.) can be observed using existing junctions, even

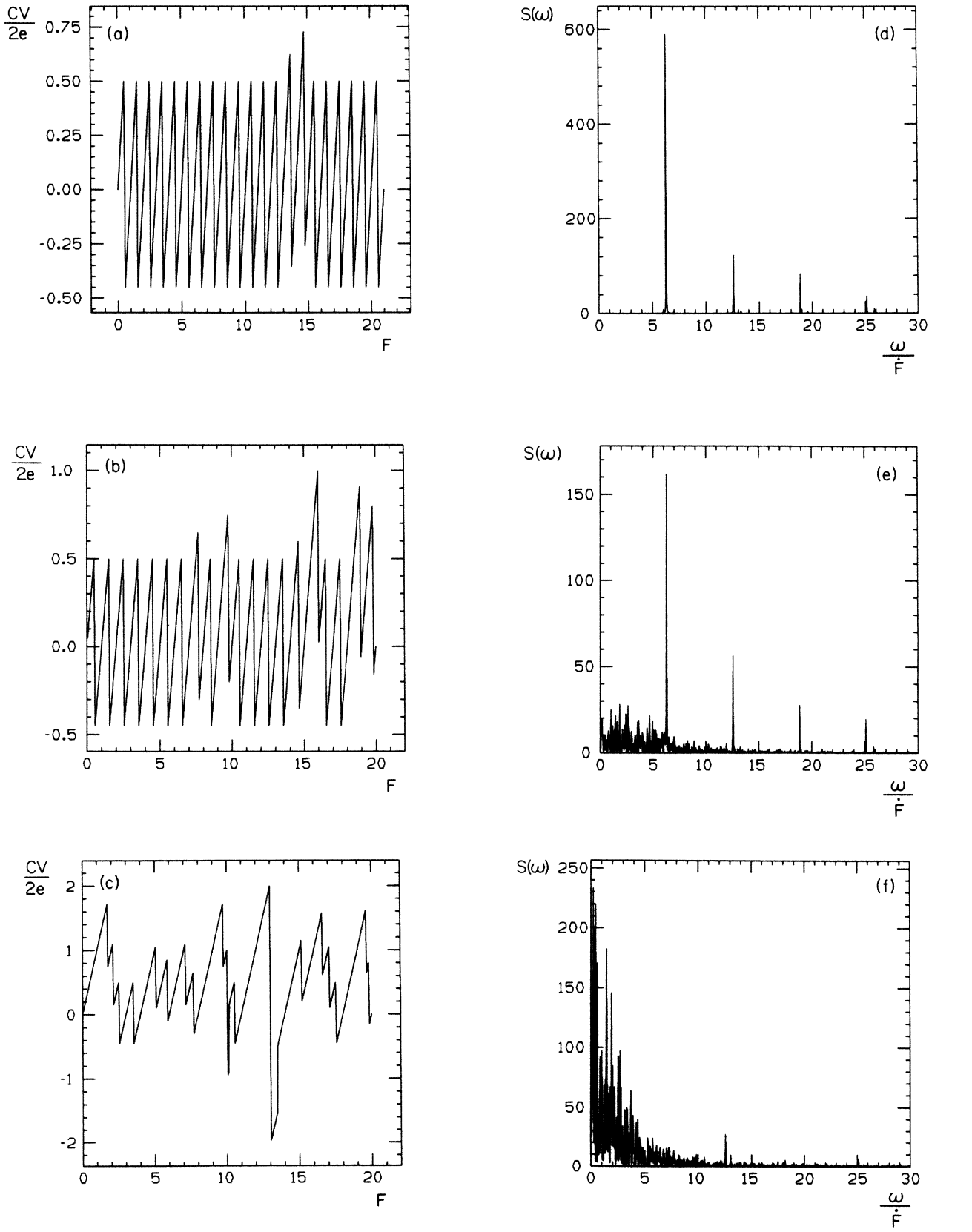

FIG. 14. Results of numerical simulations of the stochastic process described by Eq. (4.9), which includes both Zener and inelastic transitions. (a), (b), and (c) correspond to points *A*, *B*, and *C* in Fig. 13, and (d), (e), and (f) are the corresponding power spectra. The parameters are as in Fig. 13.

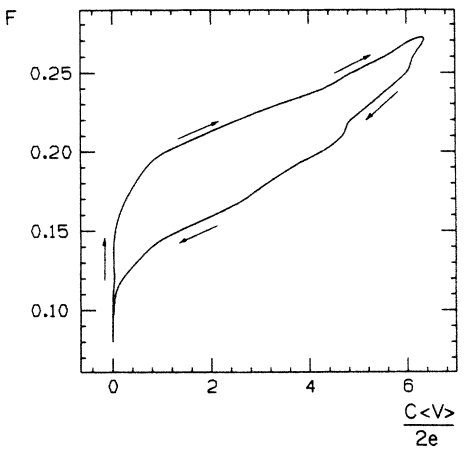

FIG. 15. Hysteretic response for case I. The average response was calculated by averaging $F(t)$ over a period $\Delta t = 6.25$ ns. The parameters are $d\dot{F}/dt = 0.5 \times 10^7$ s^{-1}, $C = 1$ fF, and $\pi E_{\rm gap}^2/4\hbar E_k = 3.125 \times 10^{10}$ Hz.

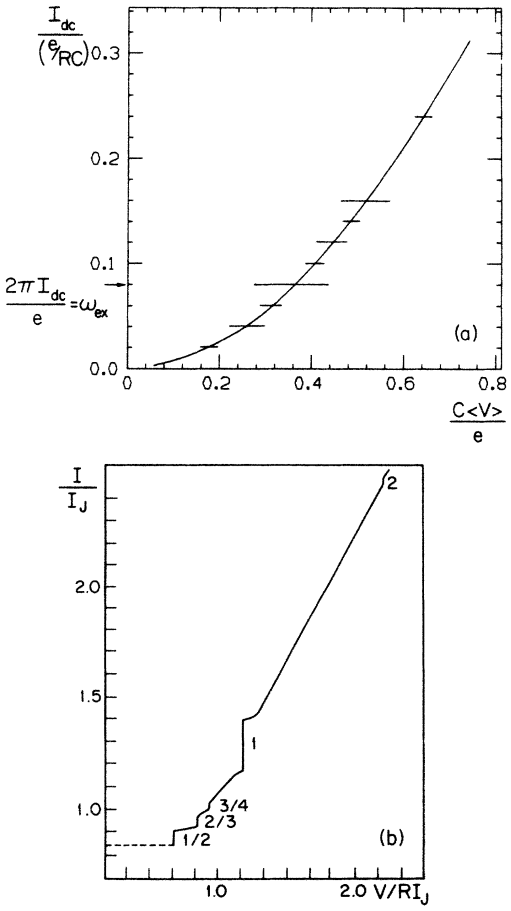

FIG. 16. (a) Schematic I-V characteristic of an ultrasmall junction in the presence of direct and alternating current as discussed in the text. (b) The I-V characteristic of a Josephson junction in the presence of microwave radiation. I_J is the Josephson critical current and ω_{ex} is the frequency of the microwave radiation.

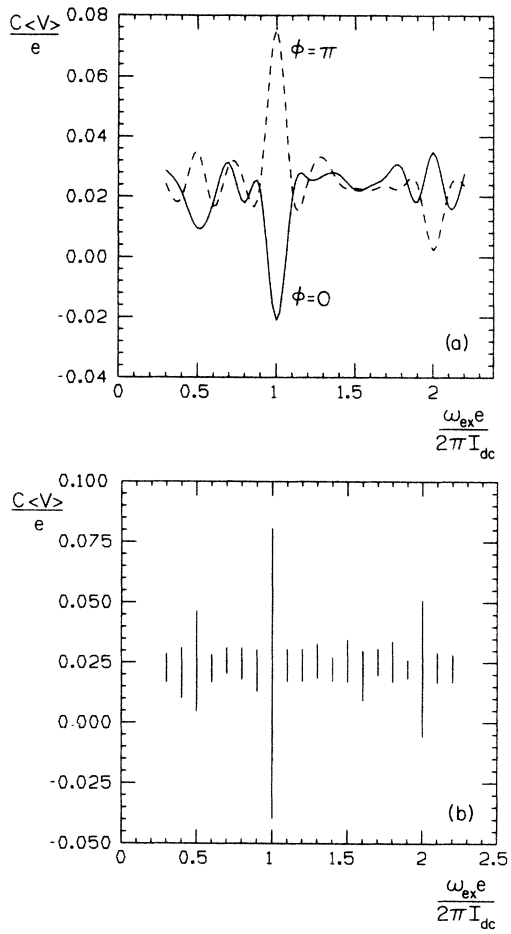

FIG. 17. (a) The average voltage as a function of the external frequency ω_{ex} for the semiclassical picture of Eq. (5.8) in the presence of a current described by Eq. (5.5). The parameters are $R_{\rm in} = 500\Omega$, $C = 1$ fF, $T = 0.05$ K, $I_{\rm dc} = 0.1$ nA, and $I_{\rm ac}/I_{\rm dc} = 0.4$. (b) The width of the subharmonic steps for the same parameters as in (a). The widths were calculated by varying ϕ in the range 0–2π.

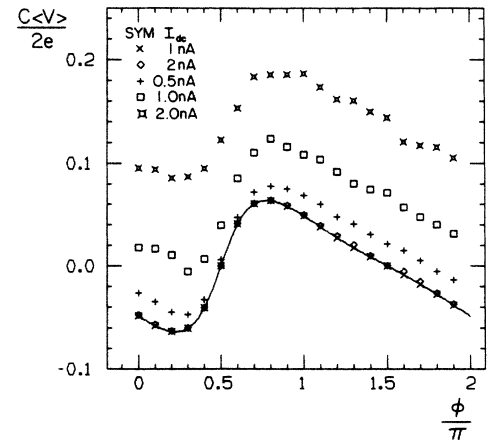

FIG. 18. The average voltage on the first harmonic step ($\omega_{ex} = 2\pi I_{\rm dc}/e$), as a function of ϕ according to the coherent picture. The parameters are $R_{\rm in} = 2500$ Ω, $C = 1$ fF, and $\pi E_{\rm gap}^2/4\hbar E_k = 0.625 \times 10^{10}$ Hz. The solid line shows the analytical approximations.

when $k_BT > e^2/2C$. As the temperature is increased $P(Q)$ broadens and its maximum is shifted towards smaller Q, as shown in Fig. 23. This shift results from the increase in $r(Q)$ shown in Fig. 24. Thus in the limit $k_BT \gg e^2/2C$ where the $e^2/2C$ shift in the Fermi distribution is negligible, $\langle V \rangle \approx RI_{dc}$. However, when the average voltage is increased such that $k_BT \ll eV$ the $e/2C$ shift in $r(Q)$ becomes large, as also shown in Fig. 24. In this limit $r(Q)$ approaches the line $(Q - e/2)/RC$ and thus has an $e/2C$ shift as in the low-temperature case as is shown in Fig. 25. This means that even at high temperatures we can observe the capacitance effect using existing junctions. The effect of temperature on the I-V characteristic is shown in Fig. 24. The shift in the I-V characteristic relative to the absolute voltage is $e/2CV$. Since eV is of the order of k_BT the ratio $e/2CV$ is approximately given by the ratio of the charging energy to the mean thermal energy, $e^2/2Ck_BT$. For example, using a junction with a capacitance of 10^{-14} F we can observe a 10% shift in the voltage (due to charging the energy) at a temperature of 1 K. Since observations can be carried out at such temperatures one can use junctions made of materials that become superconducting at lower temperatures, e.g., Al-Al_2O_3-Al junctions. Observation of a shift in the I-V characteristic will provide strong support to the existence of the predicted voltage oscillations. Positive results will give the motivation to fabricate junctions with $C = 10^{-16} - 10^{-18}$ F, which will make it possible to perform measurements in the limit $k_BT \ll e^2 2C$, so that the low-current part ($I_{dc} < e^2/2C$) of the I-V characteristic can be studied. In this limit voltage oscillations may be observable. Measurement of the I-V characteristics can also verify the prediction that for $V < e/2C$ the current is proportional to V^2.

In Sec. IV we have related the average voltage in the coherent picture to that obtained from the semiclassical approach. Moreover, for a certain range of parameters (as discussed in Sec. IV), the coherent picture predicts an hysteretic I-V characteristic with a zero-voltage step, as shown in Fig. 15.

The frequency of the Bloch oscillations (for small values of $\dot{F}$) is high, which makes experimental observation difficult. For a junction with $C = 10^{-15}$ F and $R = 1000\ \Omega$, the oscillations are observable when $I_{dc} < e/RC \equiv 1.6 \times 10^{-7}$ A, which corresponds to a frequency of 10^{12} Hz. Even if we go down to $I_{dc} = 10^{-9}$ A currents the frequency is 10^{10} Hz. To avoid this difficulty of direct measurement of the oscillations we propose to study the interference phenomena discussed in Sec. V when the junction is driven by both a direct and alternating current sources. A possible way to induce both types of current is to use an inductor and a capacitor in series and to apply an alternating flux through the inductor (e.g., by using Josephson-junction technology). These experiments may not only provide a direct verification of the existence of the Bloch oscillations but may also provide a demonstration that the junction can indeed be used as a phase-voltage converter. Finally, one has to keep in mind the intriguing possibility of quantum coherent oscillations in a Josephson junction biased with a charge e. To measure this we have to increase the bias charge to e.

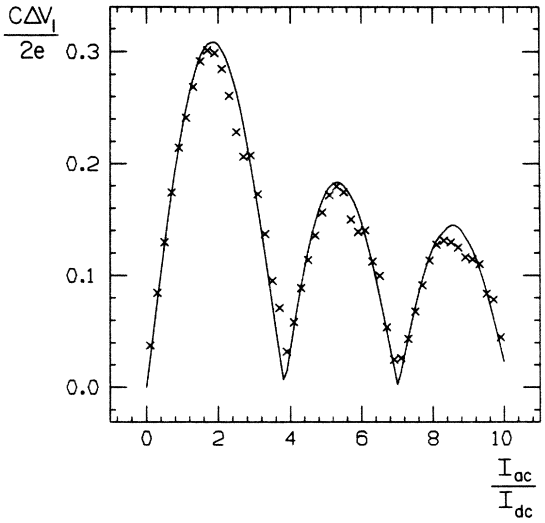

FIG. 19. The maximum width (twice the amplitude) of the first harmonic step as a function of f_{ac}/f_{dc}. The solid line is the analytical approximation in the case of no Zener transitions, and the $\times$ are the results of numerical simulations for $f_{dc} = 0.625 \times 10^9$ Hz, $\pi E_{gap}^2/4\hbar E_k = 5 \times 10^{10}$ Hz, and $R_{in} = 2000\ \Omega$.

The charge then has to be measured at various time intervals [see suggested experiments on MQC in SQUID's (Ref. 30)].

Note added. After completion of this work we became aware of experimental results on small tunnel junctions which have since been published by T. A. Fulton and G. J. Dolan, Phys. Rev. Lett. **59**, 109 (1987).

ACKNOWLEDGMENTS

We thank M. Büttiker and R. Landauer for useful discussions on the realization of a current source and for constructive comments on an early version of the manuscript. We also thank R. C. Jaklevic, A. Legget, and R. Wilkins for useful comments, and T. A. Fulton and G. J. Dolan for discussing with us their unpublished results. This research was partially supported by National Science Foundation (NSF) Grant No. DMR-86-08305, Grant No. DAAL-03-87-K-0007 from the U.S. Army Research Office, a grant from the Israel Academy for Science and Humanities, a Tel Aviv University Grant for Basic Research, and a grant from the U.S.—Israel Binational Science Foundation (BSF). Computer simulations were done in part using time granted by the NSF San Diego Supercomputer Center. One of us (K.M.) was supported by the Center for High Frequency Microelectronics at the University of Michigan. E.B.-J. and Y.G. were partially supported by Bat-Sheva grants.

APPENDIX: DESCRIPTION OF DRIVING FORCES FOR A JUNCTION

We are interested in junctions driven by an external force. In this appendix we examine various types of driving forces, their realizations, and their approximate quantum-mechanical description.

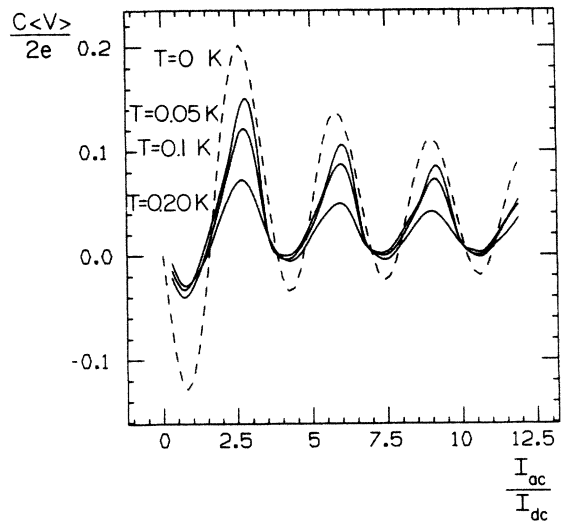

FIG. 20. The average voltage on the first harmonic step ($\omega_{ex}=2\pi I_{dc}/e$) in the semiclassical picture as a function of I_{ac}/I_{dc}. The parameters are $R_{in}=2500\ \Omega$, $C=1$ fF, $f_{dc}=0.625\times10^9$ Hz, and $\phi=0$. The dashed line shows the analytical approximations for $T=0$.

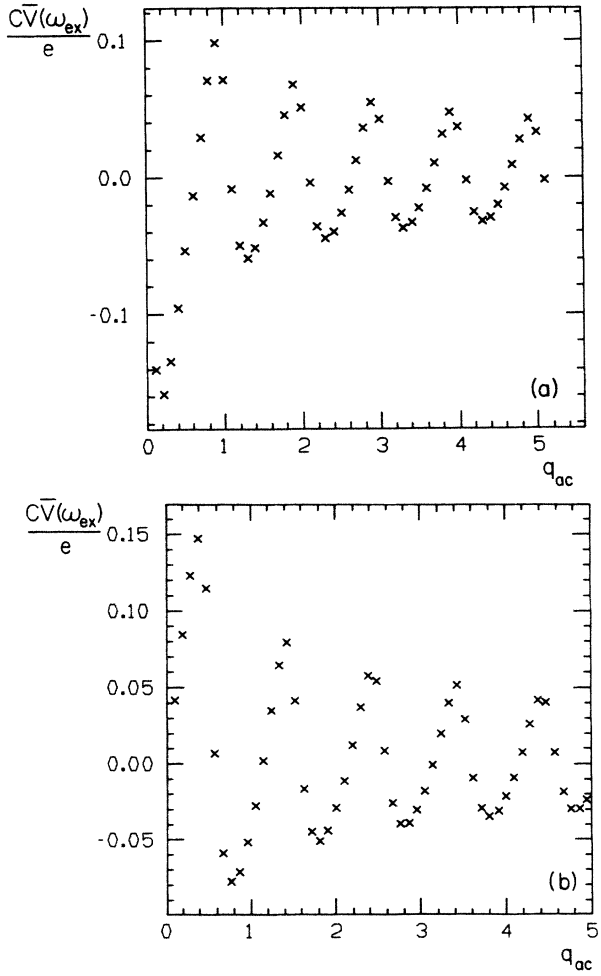

FIG. 21. $\bar{V}(\omega_{ex})$ [Eq. (5.12)] as a function of F_{ac} for the coherent picture. The parameters are $R_{in}=2500\ \Omega$, $C=1$ fF, $\pi E_{gap}^2/4\hbar E_k=0.625\times10^{10}$ Hz, and $e\gamma=1$ nA (a) for $F_{dc}=0$ and (b) for $F_{dc}=\frac{1}{2}$.

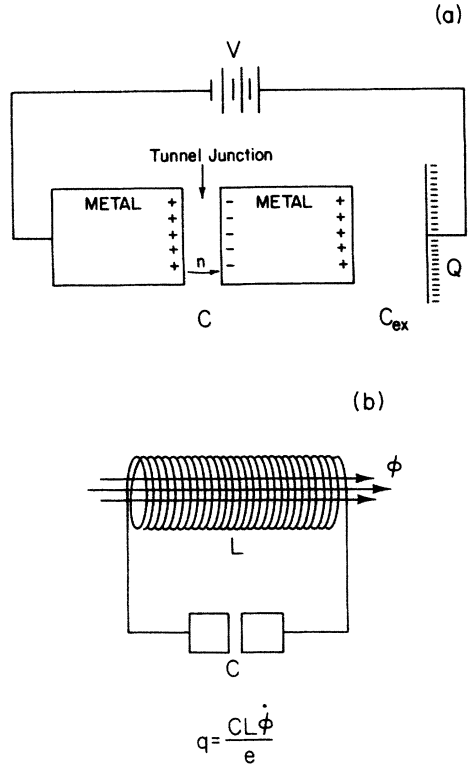

FIG. 22. (a) A configuration to induce a charge $Q=(CC_{ex}/C+C_{ex})V$ on a junction using a voltage source connected through an external capacitance C_{ex}. (b) At high frequencies the charge is induce through an inductor driven by an external flux ϕ.

It is now accepted that the dynamics of mesoscopic systems depends strongly upon the manner in which they are connected to the external world.[2] We are specifically concerned with ultrasmall capacitance junctions in which the electrostatic charging energy of a single electron, $e^2/2C$, is large. In this limit the behavior of the junction depends strongly on whether the impedance of the driving force is low, thus shorting the capacitance, or if it has

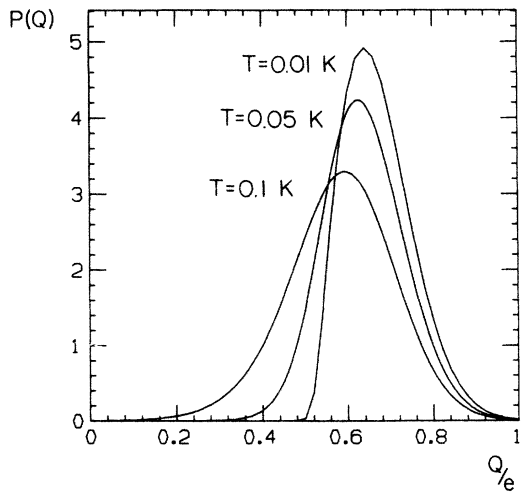

FIG. 23. The effect of temperature on $P(Q)$. The parameters are $C=1$ fF, $R=2500\ \Omega$, and $I_{dc}=1$ nA.

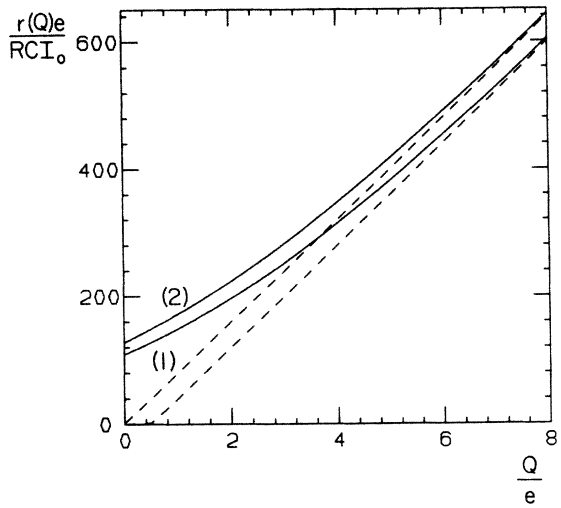

FIG. 24. Comparison of $r(Q)$ for $T=3.0$ K, $C=1$ fF, and $R=2500\ \Omega$ with (line 1) and without (line 2) the $e^2/2C$ shift discussed in the text.

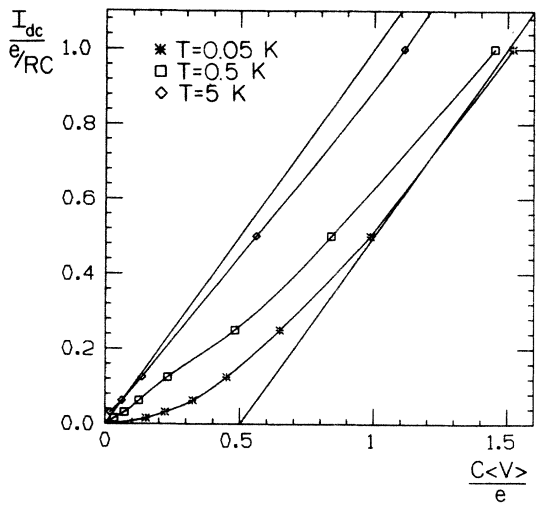

FIG. 25. The effect of temperature on the I-V characteristic in the semiclassical picture. Here $R=2500\ \Omega$ and $C=1$ fF.

high impedance, so that the charging energy is relevant. In other words, we expect a different response if the junction is connected to a voltage source (a device with zero internal impedance) or a current source (a device with infinite internal impedance). An important clue to how these two limits differ from each other is given by the study of the current and voltage fluctuations of normal junctions as discussed in Refs. 20 and 21. The power spectrum of the current noise measured in a circuit closed by an ammeter (zero internal resistance) is given by the familiar Johnson-Nyquist result[39]

$$S_I(\omega)=\frac{1}{\pi R}\hbar\omega\coth\left[\frac{\hbar\omega}{2k_BT}\right], \tag{A1}$$

where R is the resistance of the junction, defined in this paper. In contrast, if we measure the power spectrum of the voltage fluctuations using a voltmeter (infinite internal resistance) we obtain

$$S_V(\omega)=\frac{1}{\pi}\,\mathrm{Re}\left[\frac{1}{\tilde{R}(\omega)+i/\omega C}\right]\coth\left[\frac{\hbar\omega}{2k_BT}\right], \tag{A2}$$

where $\tilde{R}(\omega)$ is the resistance calculated in Ref. 21. Using the fluctuation-dissipation relation[40] we expect the response of the junction to a voltage source to be related to the current fluctuations measured by a resistanceless ammeter since in both cases the junction is shorted by the external circuit. Indeed, the average current in the presence of an external voltage source is given by V/R, where R appears in the expression for the current fluctuations in Eq. (A1). Similarly we expect that the response to a current source to be related to the voltage fluctuations.[21]

For a junction with a static external bias charge q measured in units of e, as discussed by Büttiker in Ref. 35, the Hamiltonian (neglecting the internal degrees of freedom) is

$$H=e^2/2C(q-\hat{n})^2+H_T\ , \tag{A3}$$

where $\hat{n}$ is the number operator measuring the number of elementary charges that have been transferred across the junction and H_T is the tunneling Hamiltonian. In Ref. 21 it is shown that the response to the bias charge is indeed related by the fluctuation-dissipation relations to the voltage fluctuations. A direct-current source I_{dc} corresponds to an external bias charge that increases linearly in time,

$$\dot{q}=I_{dc}/e\ . \tag{A4}$$

This result suggests that an ideal current source can be described by Eq. (A3) where q is given by Eq. (A4). We stress that in this picture the current source enters as a classical field coupled to the number operator. This is in contrast to Refs. 9 and 10 where the current source (in the case of a Josephson junction) is described as a classical field coupled to the phase operator $\hat{\theta}$, the operator conjugate to $\hat{n}$. Additional discussion of the relations between the two pictures of a current source in the presence of internal degrees of freedom is given in Ref. 38.

In Fig. 22(a) we show a simple realization of a charge source suggested first in an experiment by Lambe and Jaklevic,[41] and recently put forward by Büttiker.[35] The junction with capacitance C is connected to a voltage source V through a capacitance C_{ex}. The bias charge is given by

$$q=\frac{CC_{ex}}{C+C_{ex}}\frac{V}{e}\ . \tag{A5}$$

If V increases linearly in time this configuration provides a realization of a current source

$$I_{dc}=\frac{CC_{ex}}{C+C_{ex}}\dot{V}\ . \tag{A6}$$

This realization is useful for the study of both constant and time-dependent bias charge q.[35] We emphasize,

however, that it can represent a current source only if its impedance $(\omega C_{ex})^{-1}$ is much larger than that of the junction. At high frequencies ($\omega > 10^{12}$ Hz for $C_{ex} = 1$ fF) we can use the configuration shown in Fig. 22(b) where the junction is driven by an external inductor L_{ex}. In this latter case ωL_{ex} has to be larger than the impedance of the junction.

A voltage source is described within the framework of quantum mechanics as a constraint that imposes a difference of eV in the electrochemical potential across the junction, where eV can assume an arbitrary value. Similarly we consider a charge source that can induce an arbitrary (i.e., continuous) value of the bias charge q, where q is a c number. Throughout this paper we neglect fluctuations in q, a point that requires more detailed consideration.[42]

---

*Permanent Address: Department of Nuclear Physics, The Weitzmann Institute, 76 100, Rehovot, Israel.

[1] *Electron-Beam Lithography in Microelectronics Fabrication,* edited by B. R. Brewer (Academic, New York, 1980).

[2] For a review of mesoscopic systems, see Y. Imry, in *Memorial Volume in Honor of Professor Shang-keng Ma,* edited by G. Grinstein and G. Mazenko (World Scientific, Singapore, 1986); E. Ben-Jacob, M. Buttiker, and R. A. Webb, *Physics Today* (to be published).

[3] E. Ben-Jacob and Y. Gefen, Phys. Lett. **108A**, 289 (1985).

[4] E. Ben-Jacob, Y. Gefen, K. Mullen, and Z. Schuss, in *SQUID 85,* edited by H. D. Hahlbohm and H. Lübbig (Walter de Gruyter, Berlin, 1985).

[5] D. V. Averin and K. K. Likharev, in Ref. 4.

[6] D. V. Averin and K. K. Likharev, Low Temp. Phys. **62**, 345 (1986).

[7] E. Ben-Jacob, D. J. Bergman, B. J. Matkowsky, and Z. Schuss, Phys. Rev. B **34**, 1572 (1986).

[8] A. Widom, G. Magaloudis, T. D. Clark, H. Prance, and R. J. Prance, J. Phys. A **15**, 3877 (1982); R. J. Prance, J. E. Motton, H. Prance, T. D. Clark, A. Widom, and G. Megalaudis, Helv. Phys. Acta **56**, (1983); T. P. Spiller, J. E. Mutton,, H. Prance, R. J. Prance, T. D. Clark, in Ref. 4.

[9] A. I. Larkin, K. K. Likharev, and Yr. N. Ouchinnikov, Physica (Utrecht) **126 B+C**, 414 (1984).

[10] K. K. Likharev and A. B. Zorin, J. Low Temp. Phys. **59**, 347 (1985).

[11] N. W. Ashcroft and N. D. Mermin, *Solid State Physics* (Holt, Rinehart, and Winston, New York, 1976).

[12] C. Zener, Proc. R. Soc. London **A137**, 696 (1932).

[13] K. Mullen, E. Ben-Jacob, and Z. Schuss, in *Tunneling,* edited by J. Jortner and B. Pullman (Reidel, Dordrecht, 1986).

[14] Y. Gefen and D. Thouless (unpublished).

[15] L. Solymar, *Superconductive Tunneling and Applications* (Chapman and Hall, London, 1972).

[16] C. B. Duke *Tunneling in Solids,* edited by E. Burstein and S. Lundqvist (Plenum, New York, 1968).

[17] K. Mullen, E. Ben-Jacob, and Z. Schuss, Phys. Rev. Lett. **60**, 1097 (1988).

[18] N. C. Van Kampen, *Stochastic Processes in Physics and Chemistry* (North Holland, Amsterdam, 1981).

[19] B. J. Matkowsky, Z. Schuss, C. Knessl, C. Tier, and M. Mangel, Phys. Rev. A **29**, 3359 (1984).

[20] T. L. Ho, Phys. Rev. Lett. **51**, 2060 (1983).

[21] E. Ben-Jacob, E. Mottola, and G. Schön, Phys. Rev. Lett. **51**, 2064 (1983).

[22] A. J. Leggett, Phys. Rev. B **30**, 1208 (1984); A. J. Leggett, in Ref. 4, and references therein.

[23] L. D. Chang and S. Chakravarty, Phys. Rev. B **29**, 130 (1984); **30**, 1566 (1984).

[24] F. Guinea, V. Hakim and A. Muramatsu, Phys. Rev. B **32**, 4410 (1985).

[25] H. Grabert, P. Olschowsky, and V. Weiss, Phys. Rev. B **32**, 3348 (1985).

[26] D. Waxman and A. J. Leggett, Phys. Rev. B **32**, 4450 (1985).

[27] M. P. A. Fisher, A. T. Dorsey, Phys. Rev. Lett. **54**, 1609 (1985).

[28] A. T. Dorsey, M. P. A. Fisher, and M. S. Wartak, Phys. Rev. A **33**, 1117 (1986).

[29] F. Guinea and G. Schön, Europhys. Lett. **1**, 585 (1986).

[30] C. Tesche, in Ref. 4.

[31] R. Landauer, Phys. Rev. B **33**, 6497 (1986).

[32] G. Wannier, Physics (N.Y.) **1**, 251 (1965).

[33] K. Mullen, S. Fishman, E. Ben-Jacob, and Y. Gefen (unpublished); see also M. Büttiker and R. Landauer, Adv. Solid State Phys. **25**, 711 (1985).

[34] Y. Gefen, E. Ben-Jacob, and A. O. Caldeira, Phys. Rev. B **36**, 270 (1987).

[35] M. Buttiker, Phys. Rev. B **36**, 3548 (1987).

[36] K. Mullen and E. Ben-Jacob (unpublished).

[37] *SQUID 80,* edited by H. D. Hahlbohn and H. Lübbig (Walter de Gruyter, Berlin, 1980).

[38] W. Zwerger, A. T. Dorsey, and M. P. A. Fisher, Phys. Rev. B **34**, 6518 (1986).

[39] H. B. Callen and T. A. Welton, Phys. Rev. **83**, 34 (1951).

[40] R. Kubo, J. Phys. Soc. Jpn. **12**, 570 (1957); **17**, 975 (1962).

[41] J. Lambe and R. C. Jaklevic, Phys. Rev. Lett. **22**, 1371 (1969).

[42] A. J. Leggett (private communication).